ARMA 17 - 655

Comparison between numerical and experimental observations made in hydraulic fracturing tests

Gonçalves da Silva, B.
New Jersey Institute of Technology, Newark, NJ, United States of America
Einstein, H. H.
Massachusetts Institute of Technology, Cambridge, MA, United States of America

ABSTRACT: Hydraulic fracturing is extensively used in hydrocarbon extraction and in Engineered Geothermal Systems. However, many aspects involved in the initiation, propagation and interaction of existing and newly-created fractures are not clearly understood. Since the data obtained from real-scale stimulations provide solely indirect information on the fracturing processes, laboratory and numerical analyses play a crucial role for better understanding the mechanisms involved in the hydraulic fracturing of rocks.

This paper compares the observations made in hydraulic fracturing experiments performed on prismatic granite specimens into which two flaws were precut, with finite element analyses. Both the experiments and numerical analyses used specimens with the double-flaw geometry 2a-30-30 to which 1) only water pressure inside the flaws or 2) water pressure inside the flaws and an external vertical load were applied. Two stages of crack development, namely crack initiation and crack coalescence, and the maximum and minimum principal stresses around one of the inner flaw tips, were assessed.

When no vertical load was applied, the hydraulic macro-fractures observed experimentally are tensile, and initiate from the tip end of the studied flaw and propagate to coalesce in the bridge between inner flaw tips. The numerical model results are consistent with these observations, since high tensile principal stresses occur at the tip end of the flaw and in the bridge between flaws.

On the other hand, when a vertical load of 5 MPa was applied, the hydraulic macro-fractures observed experimentally are tensile but initiate from the upper face of the flaw tip and propagate in a vertical direction and not towards the bridge between inner flaw tips. This is also consistent with the numerical results, since maximum tensile stresses only occur at the upper face of the flaw, and both maximum and minimum principal stresses are compressive in the bridge between inner flaw tips, a condition which would not lead to the development of tensile cracks

1. INTRODUCTION

Hydraulic fracturing is extensively used in hydrocarbon extraction and in Engineered Geothermal Systems. However, the fracturing processes that occur when a rock is hydraulically fractured are not clearly understood. Since the data obtained from field stimulations provide solely indirect information on the fracturing processes, laboratory and numerical analyses play a crucial role in the better understanding of the mechanisms involved in the hydraulic fracturing of rocks. Various authors have performed hydraulic fracturing experiments using different rocks and test setups in the last decades. The main foci of their research has been on determining which conditions may produce and arrest a fracture (Teufel and Clark, 1984; Warpinsky, 1982), on measuring the pressures necessary to hydraulically propagate fractures under different stress conditions (Song et al., 2001; Zoback et al., 1977), on evaluating the scalability of the experiments conducted in the laboratory (de Pater, 1994), and on observing the impact of the stress-state on the direction of propagation of the fractures created hydraulically (Ingraham, 2016). In recent research, Gonçalves da Silva (2016) conducted hydraulic fracturing tests to study the induced seismicity and the micro- and macro-scale

fracturing processes caused by the hydraulic fracturing of granite specimens.

Much effort has also been put in numerically modeling hydraulic fracturing. Researchers have been modeling with some success hydraulic fracturing using coupled geomechanical models embedded in Finite Element (FE) codes (Settari et al., 2002; Yao, 2012; Yarushina et al., 2013; Hou et al., 2013; Qinglu and Ahmad, 2016; Huang and Ghassemi, 2016; Gonçalves da Silva and Einstein, 2014). While the FE analyses have been the most used method to numerically analyze hydraulic fracturing, other methods have been developed and used, such as the extended finite element – XFEM (Gordeliy, 2016; Abbas et al., 2016), distinct element – DEM (Munjiza, 2004; Shimizu, 2011; Zhou et al., 2016; Zhangh, 2016), boundary element – BEM (Fata, 2016; Ghassemi, 2016; Kamali and Ghassemi, 2016), extended finite difference – XFDM (Zhou and Hou, 2013), and smoothed particle hydrodynamics – SPH (Pramanik et al., 2016) methods, amongst others.

This paper compares the experimental results of hydraulic fracturing tests described in Gonçalves da Silva (2016) with the numerical results presented in Gonçalves da Silva and Einstein (2014). The hydraulic fracturing tests and the numerical analyses performed as well as the stresses used in the comparison of tests and analyses will be briefly described in Section 2 – Background. The comparison between the numerical and experimental observations will be discussed in detail in Section 3. Finally, Section 4 will present a summary and conclusion of this study.

2. BACKGROUND

2.1. Hydraulic Fracturing Experiments

The test setup described in Gonçalves da Silva and Einstein (2015) can simultaneously apply a hydraulic pressure (WP) in prefabricated, or pre-cut, flaws and a vertical load (VL) on prismatic granite specimens, as shown in Figure 1 a). One single- and five double-flaw geometries were tested with 0 MPa and 5 MPa vertical loads using image (visual) and acoustic emission monitoring. The visual observations were done with a high-speed video camera which made it possible to distinguish tensile and shear cracks as well as their order of initiation. The double-flaw geometries are defined as described in Figure 1 b). Three specimens were tested for each loading condition and flaw geometry, to guarantee consistency and repeatability of the results. The granite specimens used in the hydraulic fracturing tests were 6" high x 3" wide x 1" thick, and the flaw length and aperture were 0.5" (12.7 mm) and 0.7 mm (slightly under 1/32"), respectively, as shown in Figure 2. While the vertical load was kept constant throughout each test, the water pressure was increased in increments of approximately 0.5 MPa (Figure 3) until fractures initiated and propagated. The hydraulic pressure caused the fractures to propagate until they reached the boundaries of the specimen, which then caused the hydraulic pressure to drop. For more information about the hydraulic fracturing tests conducted, refer to Gonçalves da Silva (2016).

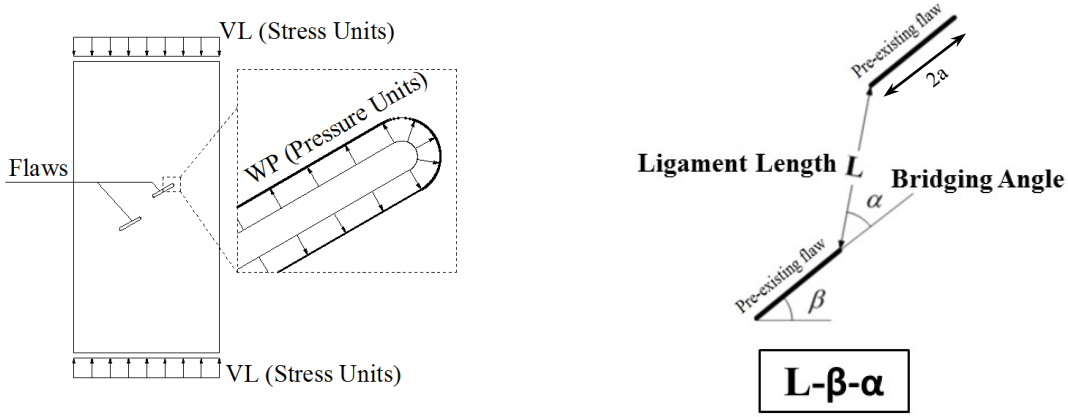

a) b)

Figure 1 - a) Loading conditions used in the hydraulic fracturing tests and b) parameters used to describe the double-flaw geometries used in the tests.

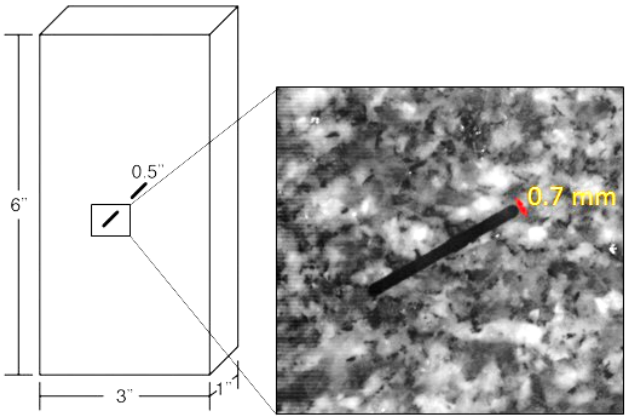

Figure 2 - Geometry of the prismatic granite specimens, including length and aperture of the flaws

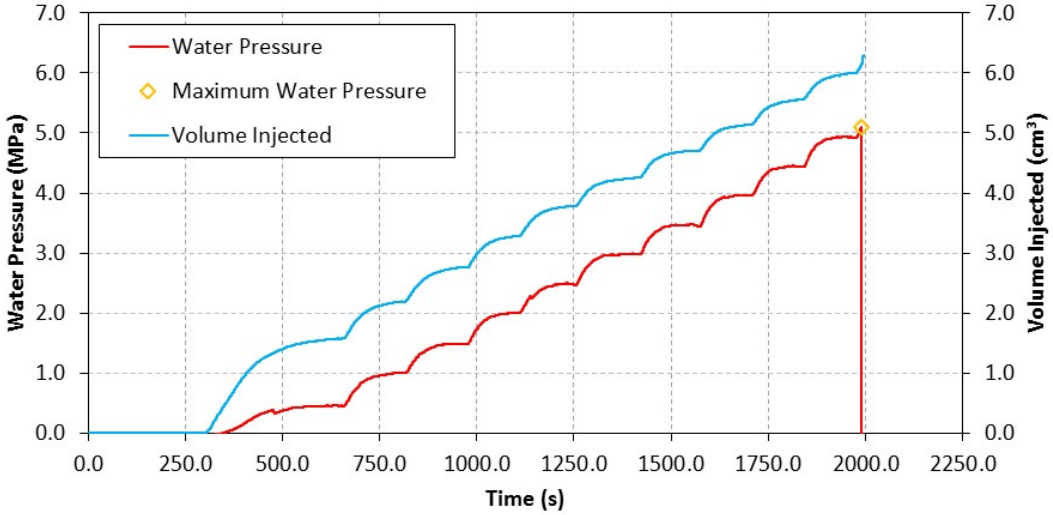

Figure 3 – Water pressure and volume of water injected vs time for the entire test

2.2. Numerical Modeling

The numerical analysis was performed with the Finite Element code ABAQUS. The geometry modeled was 2a-30-30 (Figure 4a), following the convention described in Figure 1b). The material was considered to be linearly elastic, hence this numerical analysis is only valid before any cracks initiate. The finite element mesh, shown in Figure 4 b) is much finer near the flaws, since the stresses will be concentrated in that region. The aperture of the flaws was 0.7 mm and the flaw tips were considered semi-circular, corresponding to the aperture and tip shape used in the granite specimens tested. The modeled specimen was subject to different combinations of vertical load (VL) and water pressure (WP) inside the flaws. The combinations relevant to the present comparison are shown in Table 1. It should be noted that the vertical loadings considered in the experiments and numerical model are somewhat different (see Table 1): while 0 MPa was considered for both cases, vertical loads of 5 MPa and 10 MPa were used in the experiments and numerical simulation, respectively. The difference in vertical loads (5MPa/10MPa) does not affect the numerical results presented in this paper, because one is interested in the shape of the stress field rather than in its magnitude. In fact, it is the shape of the stress field that will indicate where the cracks are expected to initiate and further propagate. Since the material is considered linearly elastic, the shape of the stress field is the same for identical ratios of WP/VL, regardless of the magnitudes of VL and WP. As shown in Table 1, the same WP/VL ratios are used for the experiments and numerical model. For more information about the model and the properties of the material used, refer to Gonçalves da Silva and Einstein (2014).

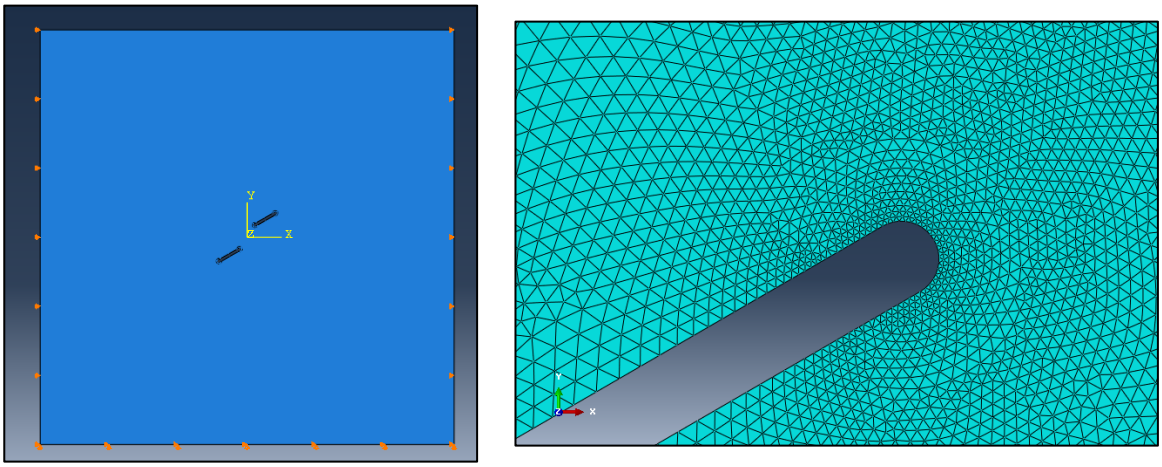

a) b)

Figure 4 – Finite Element model of geometry 2a-30-30 showing a) overall model and b) mesh near a flaw tip

Table 1 – Loading cases considered in the numerical analysis and in the experiments relevant to the present comparison

Experiments/Model	**Load Case**	**Water Pressure WP** (MPa)	**Vertical Load VL** (MPa)	**Ratio WP/VL**
Experiments	Vertical load = 0 MPa (no vertical load)	Maximum was approximately 5 MPa	0	∞
	Vertical load = 5 MPa		5	1.0
Model	Only water pressure in flaws (no vertical load)	10	0	∞
	Vertical load equal to water pressure	10	10	1.0

3. COMPARISON BETWEEN NUMERICAL AND EXPERIMENTAL OBSERVATIONS

The observations made in the hydraulic fracturing experiments for a double-flaw geometry 2a-30-30 described in Gonçalves da Silva (2016) are compared with the finite element results presented in Gonçalves da Silva and Einstein (2014). In particular, contours of the maximum principal stresses obtained from the numerical analysis are compared with the experimental observations of two stages of crack development: crack initiation and crack coalescence. Both loading conditions defined in Table 1 are analyzed, namely no vertical load applied (WP/VL=∞) and vertical load equal to water pressure (WP/VL=1). The flaws are considered to be pressurized in all cases.

3.1. Crack initiation

No vertical load (WP/VL=∞)

For the specimens tested without vertical load, tensile cracks usually initiated at the tip of the flaw, particularly from the inner flaw tips, as shown in Figure 5 a) for one of the specimens with flaw geometry 2a-30-30 and no vertical load applied. This is consistent with what was obtained in the finite element analysis for the loading condition with water pressure inside the flaws only. As shown in Figure 5 b), the maximum principal stresses are tensile around the inner flaw tip of the left flaw. The highest maximum principal stress is tensile and occurs at the tip of the flaw, where crack initiation was actually observed in the hydraulic fracturing tests with this geometry and loading conditions. This indicates that the

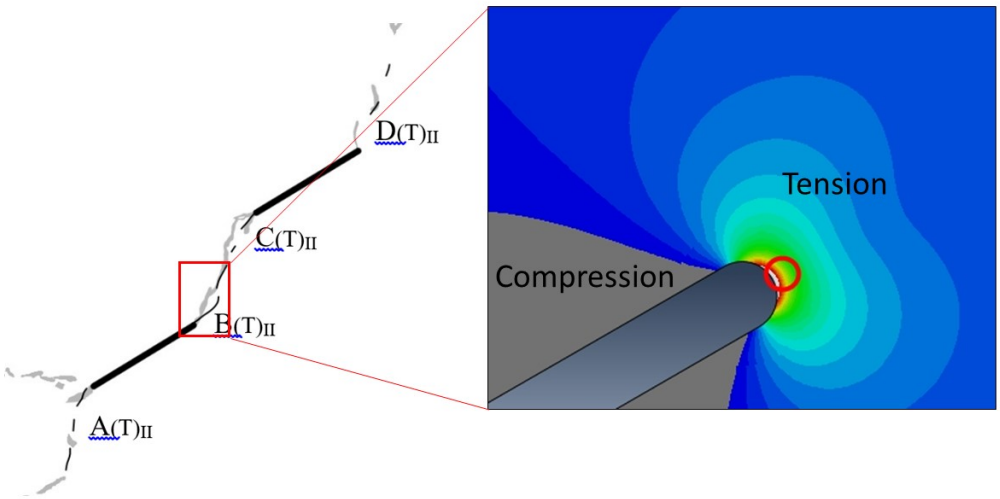

a) b)

Figure 5 - a) Crack initiation in specimen with flaw geometry 2a-30-30 without vertical load and b) maximum principal stresses contours near the tip from Finite Element analysis for WP/VL=∞. Notes: A, B, C, … represent the order of initiation of the crack; T – Tensile crack and S – Shear crack

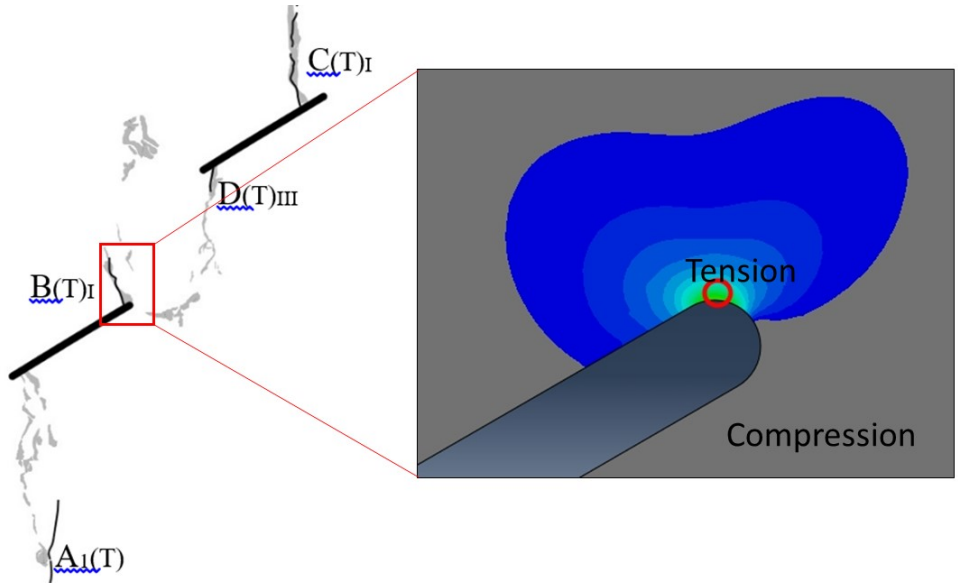

a) b)

Figure 6 - a) Crack initiation in specimen with flaw geometry 2a-30-30 with a vertical load of 5 MPa and b) maximum principal stresses contours near the tip from Finite Element analysis for WP/VL=1. Notes: A, B, C, … represent the order of initiation of the crack; T – Tensile crack and S – Shear crack

numerical results are consistent with the observed initiation of tensile cracks from the tips of the flaws.

Vertical load equal to water pressure (WP/VL=1)

For the specimens in which a vertical load of 5 MPa was applied, the cracks initiated at the upper face of the flaw tip (for the inner tip of the left flaw), as shown in Figure 6 a). This is also consistent with the numerical results shown in Figure 6 b). These contours were obtained for a ratio WP/VL = 1.0, which corresponds to the near-failure conditions for the 2a-30-30 specimens. It can be seen that there is a small bulb of positive (tensile) maximum principal stresses at the upper face of the tip under study, while the remaining area around the flaw

tip shows compressive maximum principal stresses. This numerical result indicates that a tensile crack can initiate at the upper face of the flaw tip, which actually corresponds to what was observed experimentally.

3.2. Crack Coalescence

The stress states around the flaws obtained numerically are valid to study crack initiation, since the model considers linearly elastic behavior of the material. However, once a first crack initiates the stresses change, and crack propagation and coalescence can not be interpreted accurately using the stress contours presented in this Subsection. Nevertheless, in the context of the comparison between the experimental and numerical results, the linear elastic stresses will be used to better understand the reasons why the observed coalescence occurred.

No vertical load (WP/VL=∞)

For the specimens tested without a vertical load, a direct coalescence of tensile cracks was observed connecting the inner tips of the flaws, as shown in Figure 7 a). The circle in the figure indicates the location where crack coalescence took place. The numerical model shows that the entire bridge between flaw tips is subject to tensile maximum principal stresses. This stress state is consistent with the propagation of the tensile cracks that linked the inner tips of the flaws observed in the hydraulic fracturing experiments.

Vertical load equal to water pressure (WP/VL=1)

The specimens tested with a vertical load of 5 MPa show cracks developing upwards, from the inner tip of the left flaw and the outer tip of the right flaw, and downwards, from the outer tip of the left flaw and inner tip of the right flaw. Consequently, coalescence does not take place in the bridge between inner flaw tips, as shown in Figure 8 a). The reason why there are no cracks propagating towards the bridge between inner flaw tips is that this region is subject to compressive maximum principal stresses, as shown in Figure 8 b). Having compressive maximum principal stresses means that the minimum principal stresses are also compressive (as illustrated in Figure 9 in the left Mohr circle, since the maximum principal stress is compressive, the minimum principal stress must also be compressive because it has to be equal or smaller than the maximum principal stress). Because of this, it is not possible to have tensile cracks propagating to the bridge between inner flaw tips; it is, in fact, more likely that the tensile cracks that initiated at the upper face of the inner flaw tip under study follow the direction of initiation and propagate vertically to the ends of the specimen, as was observed in the experiments.

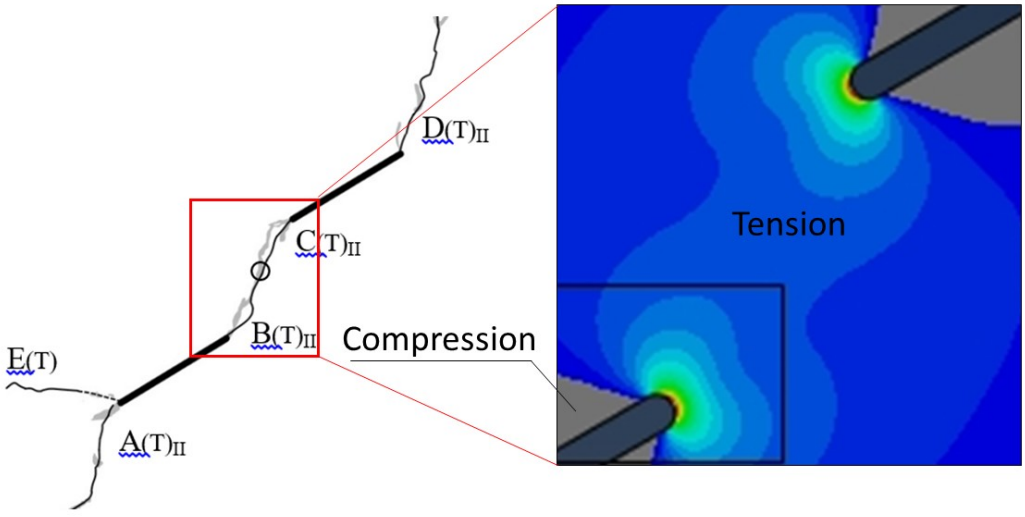

a) b)

Figure 7 - a) Direct crack coalescence in specimen with flaw geometry 2a-30-30 without vertical load and b) maximum principal stresses contours in the bridge between tips from Finite Element analysis for WP/VL=∞. Notes: A, B, C, … represent the order of initiation of the crack; T – Tensile crack and S – Shear crack

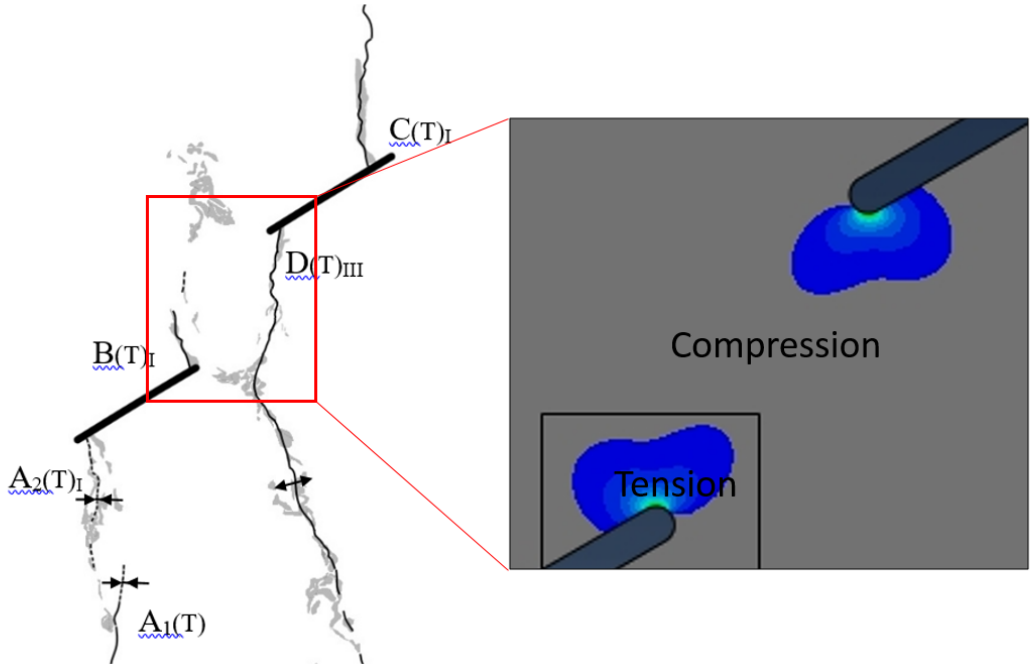

a) b)

Figure 8 - a) No coalescence between inner flaw tips in specimen with flaw geometry 2a-30-30 with a vertical load of 5MPa and b) maximum principal stresses contours in the bridge between tips from Finite Element analysis for WP/VL=1. Notes: A, B, C, … represent the order of initiation of the crack; T – Tensile crack and S – Shear crack

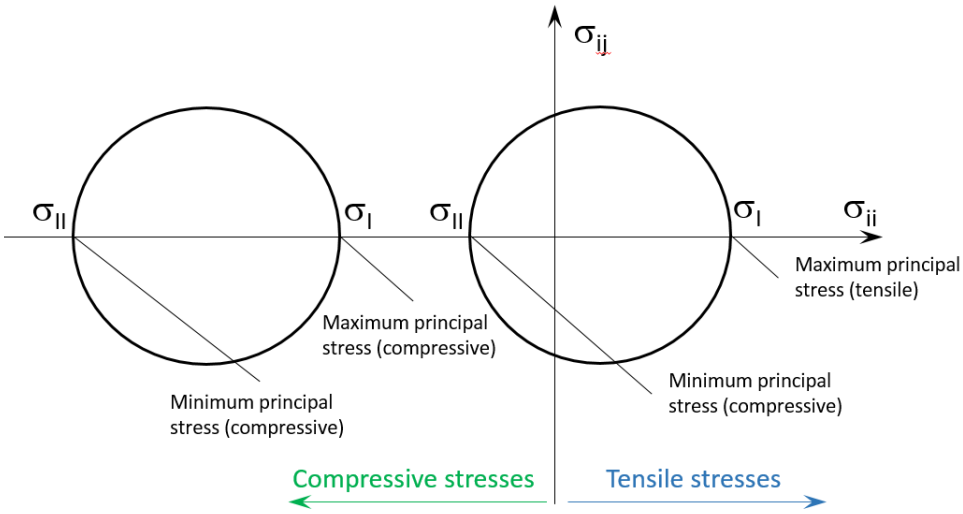

Figure 9 – Mohr circles for stress conditions with compressive maximum and minimum principal stresses (left Mohr circle) and with tensile maximum and compressive minimum principal stresses (right Mohr circle)

4. SUMMARY AND CONCLUSION

The results of the numerical analysis performed using the double-flaw geometry 2a-30-30 are consistent with what was observed in the hydraulic fracturing tests for the same geometry. For the specimens to which no vertical load was applied (WP/VL = ∞), the numerical model shows that tensile cracks developing from the inner flaw tips are likely to initiate from the tip end, then propagate and coalesce in the bridge between inner flaw tips. This corresponds to what was observed in the hydraulic fracturing experiments. For the specimens on which a vertical load of 5 MPa (WP/VL≈1) was applied, the numerical analysis indicates that tensile cracks are likely to initiate from the upper face of the inner flaw tip (for the inner tip of the left flaw), since it is the sole place where tensile stresses occur. These tensile cracks are then unlikely to propagate towards the bridge between inner flaw tips, since both maximum and minimum principal stresses are compressive in that region. It is more likely that the cracks follow the direction of initiation and therefore propagate in a vertical direction. This is also consistent to what was observed experimentally.

This paper shows a comparison between experimental observations and numerical modeling results. The findings presented may be used in the future as the basis for further developments and validation of coupled hydro-mechanical models used to simulate the hydraulic fracturing of rocks.

5. ACKNOWLEDGEMENTS

The authors would like to acknowledge the support of this research by TOTAL in the context of the project Multi-scale Shale Gas Collaboratory and by the MIT Energy Initiative. Both entities not only provided financial support but also contributed through constructive technical discussions.

REFERENCES

Abbas, S., Gordeliy, E. and Peirce, A. (2016) Modeling multiple curved fractures connected through a wellbore using a fluid-coupled XFEM algorithm. 50th US Rock Mechanics / Geomechanics Symposium held in Houston, Texas, USA, 26-29 June 2016. American Rock Mechanics Association. ARMA 16-32

Cheng, Q. and Ghassemi, A. (2016) Numerical Modeling of Newberry EGS Stimulation. 50th US Rock Mechanics / Geomechanics Symposium held in Houston, Texas, USA, 26-29 June 2016. American Rock Mechanics Association. ARMA 16-69

de Pater, C.J., Cleary, M.P., Quinn, T.S., Barr, D.T., Johnson, D.E. and Weijers, L. (1994) Experimental Verification of Dimensional Analysis for Hydraulic Fracturing. SPE 24994. SPE Production and Facilities. Society of Petroleum Engineers. 9(4): 230-238

Fata, S.Nintcheu (2016) Coupling elasticity and fluid flow for a 3D hydraulic fracturing solver. 50th US Rock Mechanics / Geomechanics Symposium held in Houston, Texas, USA, 26-29 June 2016. American Rock Mechanics Association. ARMA 16-506

Ghassemi A. (2016) Impact of Fracture Interactions, Rock Anisotropy and Heterogeneity on Hydraulic Fracturing: Some Insights from Numerical Simulations. 50th US Rock Mechanics / Geomechanics Symposium held in Houston, Texas, USA, 26-29 June 2016. American Rock Mechanics Association. ARMA 16-0283

Gonçalves da Silva, B. and Einstein, H. (2014) Finite Element study of fracture initiation in flaws subject to internal fluid pressure and vertical stress, International Journal of Solids and Structures, 51(23-24):4122-4136

Gonçalves da Silva, B. (2016) Fracturing processes and induced seismicity due to the hydraulic fracturing of rocks. PhD Thesis, Massachusetts Institute of Technology

Gordeliy, E., Abbas, S. and Prioul, R. (2016) Modeling of near-wellbore fracture reorientation using a fluid-coupled 2D XFEM algorithm. 50th US Rock Mechanics / Geomechanics Symposium, Houston, Texas, USA, 26-29 June 2016. American Rock Mechanics Association. ARMA16-494

Hou, Z.M., Zhou, L. and Kracke, T. (2013) Modelling of seismic events induced by reservoir stimulation in an enhanced geothermal system and a suggestion to reduce the deformation energy release. Rock Dynamics and Applications – State of the Art, 161-175. Taylor and Francis Group, London, United Kingdom

Huang, K. and Ghassemi, A. (2016) A Coupled Nonlocal Damage Model for Hydraulic Fracture Propagation. 50th US Rock Mechanics / Geomechanics Symposium held in Houston, Texas, USA, 26-29 June 2016. American Rock Mechanics Association. ARMA16-131

Ingraham, M.D., Bolintineau, D., Rao, R.R., Bauer, S.J., Quintana, E.C. and Lechman, J.B. (2016) Laboratory Scale Hydraulic Fracture of Marcellus Shale. 50th US Rock Mechanics / Geomechanics Symposium held in Houston, Texas, USA, 26-29 June 2016. American Rock Mechanics Association. ARMA 16-0085

Kamali, A. and Ghassesi, A. (2016) On the Reservoir Stimulation Mechanisms in Fractured Reservoirs. 50th US Rock Mechanics / Geomechanics Symposium held in

Houston, Texas, USA, 26-29 June 2016. American Rock Mechanics Association. ARMA 16-851

Munjiza (2004) The Combined Finite-Discrete Element Method. Wiley

Settari, A., Sullivan, R.B., Walters, D.A. and Wawrzynek, P.A. (2002) 3-D analysis and prediction of microseismicity in fracturing by coupled geomechanical modeling. Society of Petroleum Engineers. SPE-75714-MS

Shimizu, H., Murata, S. and Ishida, T. (2011) The distinct element analysis for hydraulic fracturing in hard rock considering fluid viscosity and particle size distribution. International Journal of Rock Mechanics and Mining Sciences. 48(5): 712–727

Song, I., Suh, M. and Won, K.S. (2001) A laboratory study of hydraulic fracturing breakdown pressure in tablerock sandstone Geosciences Journal. 5: 263

Teufel, L. W. and Clark, J. A. 1984. Hydraulic Fracture Propagation in Layered Rock: Experimental Studies of Fracture Containment. SPE Journal 24 (1): 19-32. SPE9878-PA.

Warpinsky, N.R., Clark, J.A., Schmidt, R.A. and Huddle, C.W. (1982) Laboratory Investigation on the Effect of In-Situ Stresses on Hydraulic Fracture Containment. Society of Petroleum Engineers Journal. Society of Petroleum Engineers. SPE-9834-PA

Yao, Y. (2012) Linear elastic and cohesive fracture analysis to model hydraulic fracture in brittle and ductile rocks. Rock Mechanics and Rock Engineering. 45:375-387

Yarushina, V.M., Bercovici, D. and Oristaglio, M.L. (2013) Rock deformation models and fluid leak-off in hydraulic fracturing Geophysical Journal International, 194(3): 1514-1526

Zhang, F. and Mack, M. (2016) Modeling of Hydraulic Fracture Initiation from Perforation Tunnels using the 3D Lattice Method. 50th US Rock Mechanics / Geomechanics Symposium held in Houston, Texas, USA, 26-29 June 2016. American Rock Mechanics Association. ARMA 16-534

Zhou L, Hou MZ (2013) A new numerical 3D-model for simulation of hydraulic fracturing in consideration of hydro-mechanical coupling effects. International Journal of Rock Mechanics and Mining Sciences. 60: 370–380

Zhou, J., Huang, H. and Deo, M. (2016) Simulation of Hydraulic and Natural Fracture Interaction Using a Coupled DFN-DEM Model. 50th US Rock Mechanics / Geomechanics Symposium held in Houston, Texas, USA, 26-29 June 2016. American Rock Mechanics Association. ARMA 16-739

Zoback, M.D., Rummel F., Jung R., Alheid H.J., and Raleigh C.B. (1977) Rate controlled hydraulic fracturing experiments in intact and pre-fractured rock, International Journal of Rock Mechanics and Mining Science & Geomechanics Abstracts. 14: 49-58